Letter

Visualization of Metasurface Eigenmodes with Magnetic Resonance Imaging

Alexey P. Slobozhanyuk[1,*] Alena V. Shchelokova,[1] Alexander V. Kozachenko,[1]
Irina V. Melchakova,[1] Alexander J.E. Raaijmakers,[2] Cornelis A.T. van den Berg,[2]
Pavel A. Belov,[1] and Andrew G. Webb[3]

[1]*School of Physics and Engineering, ITMO University, St. Petersburg 197101, Russia*
[2]*Department of Radiotherapy, University Medical Center Utrecht, P.O. Box 85500, 3508 GA Utrecht, Netherlands*
[3]*C.J. Gorter Center for High Field MRI, Department of Radiology, Leiden University Medical Center, Leiden, Netherlands*

The ability to control the electromagnetic near field with metasurfaces offers potential applications over the frequency range from radio frequency to optical domains. In this work, we show an essential feature of metasurfaces, subwavelength field confinement via excitation of a large number of eigenstates in a narrow frequency range, and demonstrate an innovative way of visualizing profiles of metasurface eigenmodes with the aid of a magnetic resonance imaging (MRI) system. We show that by tuning different eigenmodes of the metasurface to the Larmor frequency, we can passively tailor the near-field distribution to adjust the desired pattern of radio-frequency excitation in a MRI experiment. Our work demonstrates a practical nonperturbed rapid way of imaging metasurface eigenmodes.

The developments of artificially designed metamaterials [1] and their two-dimensional analogs metasurfaces [2] with smaller periodicity to the wavelength have resulted in new degrees of freedom for electromagnetic field manipulation in the near-field zone. Typically composed of humanmade periodic systems with subwavelength inclusions (meta-atoms), these artificial materials can replace conventional materials with more limited electromagnetic properties. Various structures have been proposed to guide electromagnetic waves in the near-field zone [3], to design unconventional waveguides with subwavelength dimensions [4–6] and topological protection [7], and to implement geometry-invariant resonant structures [8] or compact cavities that exhibit simultaneously very high quality factors and ultralow-volume modes [9,10].

In the far-field zone, metamaterials and metasurfaces can be experimentally characterized by analyzing transmission, absorption, and reflection spectra. In the near field, special scanning techniques are usually employed to characterize eigenmodes' field distribution. The standard techniques for imaging the near field are based on collecting the signal from various spatial positions via a probe antenna mounted on a motorized platform. This mechanism was employed to image the near field of different metasurface eigenmodes in the microwave [11], infrared [12], and optical [13] frequency ranges. Typically, such

a procedure is slow, and only two-dimensional near-field profiles can be measured in one scan. Here we propose an innovative way of visualizing and studying profiles of metasurface eigenmodes with the aid of a magnetic resonance imaging (MRI) system. We employ a resonant metasurface supporting a large number of eigenmodes in a narrow frequency range and demonstrate that by changing the host material's permittivity dynamically, we can tune different metasurface eigenmodes to the Larmor frequency, and, in this way, we can visualize it with a MRI machine. While the modes of conventional dielectric resonators filled with distilled water have been visualized with the MRI system previously [14–16], the present work is aimed at demonstrating excitation of different metasurface eigenmodes and their visualization with a MRI system.

MRI is itself a near-field control technique that operates at subwavelength dimensions; the spatial resolution is not wavelength dependent but rather is limited by the encoding strength of the magnetic field gradients. The signal-to-noise ratio of MR images depends on the spatial distribution of electric and magnetic fields of the radio-frequency (rf) transmit and receive coils [17]. MRI systems work over a frequency range of tens to several hundreds of megahertz, with a typical clinical 1.5-T system operating at approximately 64 MHz. It employs a large "body coil" located in the magnet's bore for rf transmission, meaning that the electromagnetic field is deposited in all parts of the body, not only in the region of interest. Metasurfaces

---

*a.slobozhanyuk@metalab.ifmo.ru

have been used in various aspects of MRI, e.g., to improve element decoupling [18], to boost local transmit efficiency [19–23], and to enhance receive sensitivity [24–27].

A generic example of metasurfaces for MRI is schematically depicted in Fig. 1(a). Several identical thin resonant metasurfaces are placed inside the MRI machine on the patient table. By varying the permittivity of the host material of the metasurfaces, it is possible to tune different eigenmodes (of both higher and lower order) simultaneously to the Larmor frequency. These eigenmodes are characterized by the magnetic field's various distributions with the different number of nodes distributed at subwavelength scale [see, for example, Fig. 1(a)].

In this work, we consider a resonant metasurface realized as an array of 14×2 identical resonant metallic wires embedded in a host material with high permittivity ε. The length (L) of each wire is chosen to approximately satisfy

the Fabry-Perot condition for the first eigenmode at the operating frequency of the 1.5-T MRI system. Through the strong coupling of several identical resonators placed in the vicinity of each other, the original resonance frequency splits into several bands, which correspond to the different eigenstates of the metasurface resonators [9,24]. The eigenmode order can be defined as $N + 1$, where N is the number of nodes of the magnetic field (B_y component) along with the directions orthogonal to the wires [either z or x for the blue and dark blue metasurfaces shown in Fig. 1(a), respectively]. Note that since the metasurface enhances both field components orthogonal to the wire, the magnetic field amplitude's absolute value is relatively uniform for all modes. However, since only B_x and B_y components contribute to the circularly polarized rf magnetic field B_1^+ produced by the body coil, it is possible to minimize the metasurface contribution to B_x by arranging
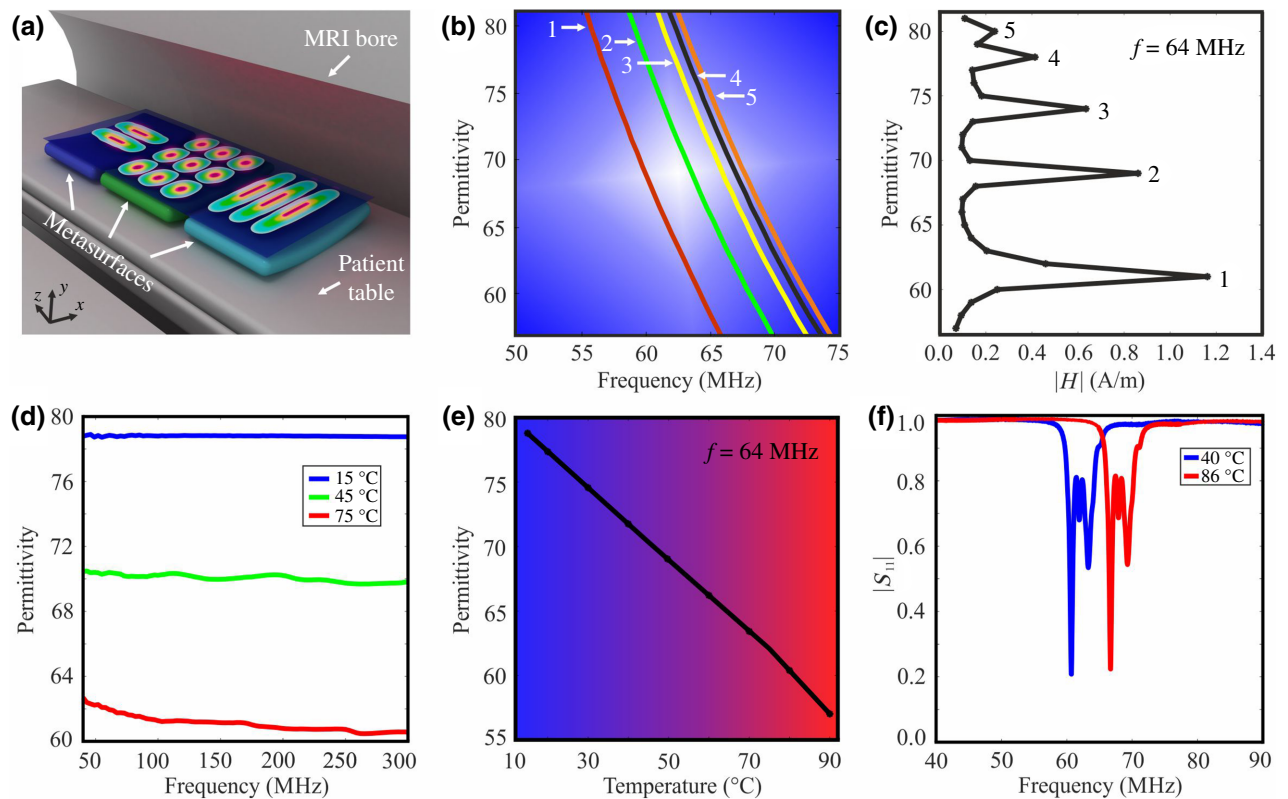

FIG. 1. (a) A schematic of various subwavelength eigenmodes in the region of space close to the specifically designed metasurfaces within the MRI bore. (b) Numerically calculated spectral dependence of the wire metasurface eigenmode frequencies as a function of the background permittivity. The numbers correspond to the mode numbers. The metasurface is excited by a plane wave with the electric field polarized along the wires. The metasurface parameters are: a 14×2 array, wire length $L = 255$ mm, period $a = 10$ mm, and radius $r = 1$ mm. The brass wires are placed in a dielectric material with variable permittivity. (c) The magnetic field amplitude averaged along the transverse direction at a 10-mm distance from the wires. The first maxima correspond to five eigenmodes of the metasurface excited at the fixed frequency of 64 MHz, which is the operating frequency of a 1.5-T MRI system for different values of the background permittivity. (d) Measured frequency dependence of real part of distilled water permittivity. The three curves correspond to different temperatures of the water. (e) The water permittivity as a function of temperature at $f = 64$ MHz. (f) The experimentally measured reflection coefficient of the loop antenna placed above the metasurface inserted in water for two different values of temperature.

the wires along the x direction, and in this way only the B_y component of the magnetic field contributes to B_1^+. The modulation in the near field can be observed in Fig. S1 within the Supplemental Material [28].

The numerically calculated dependence of the eigenmode frequencies as a function of metasurface host material permittivity is shown in Fig. 1(b) [28]. A reduction of ε shifts the eigenmodes to higher frequencies. It is interesting to note that for a properly optimized metasurface design, all considered eigenmodes can be tuned precisely to 63.8 MHz for a certain permittivity of the host material [Fig. 1(c)]. To implement such a dynamic tuning of the host material permittivity in a broad frequency range, here we rely on the temperature dependence of the permittivity of distilled water [29,30]. Figure 1(d) shows several dispersion curves measured at different temperatures of the water. The permittivity decreases with increasing temperature at the operational frequency of 63.8 MHz [Fig. 1(e)].

To confirm the tunability of the metasurface eigenmodes, we fabricate a prototype and place it in a tank filled with hot water [28]. We place a small untuned magnetic loop under the metasurface in the center and analyze the source reflection coefficient S_{11} on a vector network analyzer: the probe couples to the structure's eigenmodes,

which results in several minima in S_{11} [Fig. 1(f)]. The difference in coupling efficiency to certain eigenmodes can be explained due to the symmetry of the eigenmode and the fixed position of the loop. It is interesting to note that the eigenmodes' spectral position is strongly dependent on the temperature of the water. While initially, for the hot water [red curve Fig. 1(f)], the lowest eigenmode has a frequency just below 70 MHz, it shifts to approximately 61 MHz as the water cools, and all the eigenmodes experience a shift to lower frequencies. That confirms the possibility of tuning metasurface properties by varying the temperature of the water.

The next step is to visualize the eigenmodes' profiles via imaging of a homogeneous water phantom with the body coil used in transmit-receive mode [31]. An image representing the entire three-dimensional rf magnetic field pattern, including magnitude and phase, can be obtained within 81.6 s with a spatial resolution of 1 mm. The metasurface is inserted in the tank with hot distilled water, which is placed inside the scanner in such a way that the wires are perpendicular to the static magnetic field (along x direction). Standard gradient-echo imaging is performed every 2 min for 2 h. Initially, the water is hot, and the permittivity is relatively low ($\varepsilon \approx 62$), which allows tuning the first metasurface eigenmode to the Larmor frequency.
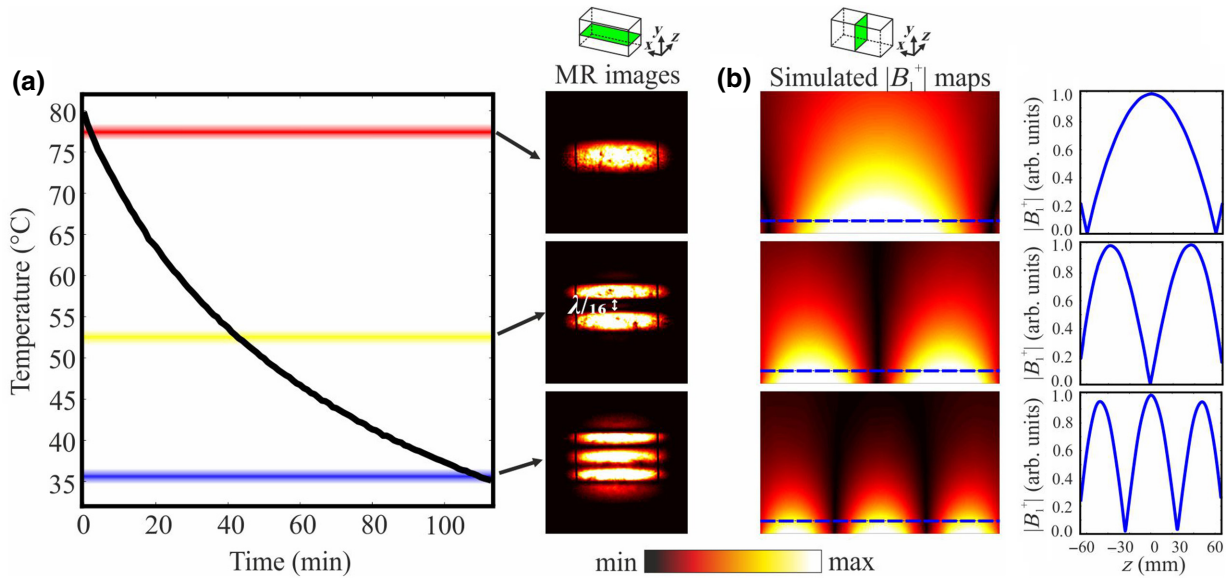

FIG. 2. Experimental demonstration of subwavelength control of the magnetic field via excitation of metasurface eigenmodes in the MRI environment. (a) The metasurface is placed in the center of the box filled with hot distilled water with wires oriented along the x axis (perpendicular to the static magnetic field B_0). A curve demonstrates the measured temperature of the water as a function of time. Three shaded areas correspond to temperatures at which the MR images are acquired. The images are acquired in the plane of the region of interest at a height of 3 cm from the metasurface for different water tank temperatures, corresponding to $76 - 77\,°C$, $53 - 54\,°C$, and $35 - 36\,°C$, respectively. The distances between two maxima in the image intensities acquired at the second mode are subwavelength and equal to approximately $\lambda/16$, where λ is the wavelength in the water. (b) Numerically calculated magnetic field profiles ($|B_1^+|$) excited by the MRI radio-frequency source coil orthogonal to the region-of-interest plane (see the top inset) for three different eigenmodes supported by the metasurface. The right-hand panels represent the modulation in the excitation field ($|B_1^+|$) in the region of interest shown by the purple lines in the left-hand panels.

Figure 2(a) shows that for a temperature of the water of approximately $76 - 77\ ^\circ$C, only one maximum can be observed above the metasurface, which corresponds to the excitation of the first eigenmode. It is characterized by a cosine shape of the rf magnetic field ($|B_1^+|$) along the metasurface [32] and has an almost homogeneous pattern in the direction orthogonal to the wires [see Fig. 2(b)]. Subsequently, the water temperature decreases to $53 - 54\ ^\circ$C while the permittivity increases. This fact effectively tunes the structure to the second eigenmode, characterized by two maxima. The MR signal is zero in the central region. Cooling to $35 - 36\ ^\circ$C realizes tuning of the third eigenmode of the metasurface to the operational frequency of MRI [Fig. 2(a), bottom panel]. The third mode is characterized by three maxima and two minima of the MR signal in the region of examination [see also $|B_1^+|$ profile in Fig. 2(b)]. As was shown previously by several groups, the first metasurface eigenmode with a homogeneously enhanced rf magnetic field in the area of examination can be employed to increase the transmit efficiency by wireless induction [25,32]. Due to the magnetic field's modulation, the higher-order modes are not relevant for conventional MRI examinations where the rf magnetic field should be as homogeneous as possible. However, specific examinations can be required to minimize MR signal for a particular area, for example, excluding or "cloaking" regions that generate motion artifacts (e.g., the aorta).

Figure 3(a) shows a three-dimensional "MRI" pattern made from Styrofoam material placed on top of the metasurface and inserted into the tank with the hot water. While no signal arises from the Styrofoam material due to the absence of hydrogen nuclei, the presence of water around the "MRI" word allows us to distinguish the shape of the letters. We acquire two images for different temperatures of the water corresponding to two particular regimes of metasurface operation. For the first regime, the background material's permittivity is such that only the first eigenmode of the metasurface contributes to the rf magnetic field in the region of interest [see Fig. 3(b)]. Therefore, the rf magnetic field is homogeneous in the region of interest, and it is possible to distinguish the "MRI" word. For the second

regime, the background's permittivity allows us to tune the second eigenmode to the Larmor frequency [Fig. 3(b)], characterized by a minimum of the magnetic field in the central part. Since the MR signal is proportional to $\sin(B_1^+)$ and the $|B_1^+|$ field is almost zero in this region, a substantial reduction of rf signal occurs, and the "MRI" word becomes invisible. This experiment is a good demonstration of the near-field control capability by a metasurface.

In summary, we have demonstrated an innovative way of visualizing and studying the spatial profiles of different eigenmodes of a metasurface with the aid of a MRI system. By dynamically changing the host material permittivity, different metasurface eigenmodes can be tuned to the Larmor frequency. In this way, we can potentially tailor the pattern of rf excitation in a MRI system, for example, to obtain a homogeneous rf magnetic field in a region of interest or to minimize signal from undesirable spatial regions that are very important for specific MRI examinations. We note that not all the metasurface eigenmodes can be used for practical MRI applications since conventional MRI requires a homogeneous distribution of B_1^+. We suggest using the inhomogeneous pattern of some of the metasurface eigenmodes to partially image a region of interest and exclude, for example, image regions that show motion artifacts. In a conventional case, this application can be implemented with a "smart" distribution of an array of surface coils, requiring a proper combination of phases and amplitudes. However, it can also be realized by a combination of a single coil and a metasurface with the consequent reduction in the number of channels required for the study. In this case, one could dynamically switch the metasurface eigenmodes using nonlinear elements (e.g., pin diodes) to switch between eigenmodes electronically. Also, for practical applications, the metasurface can be realized using printed circuit board technology. The local increase in transmit efficiency provided by the metasurface reduces the required power to produce a given B_1^+ field but does indeed introduce a spatially dependent flip angle and hence image intensity and contrast. Thus, use of a metasurface is ideal when localized image enhancement of surface features is desired. Alternatively, one can use
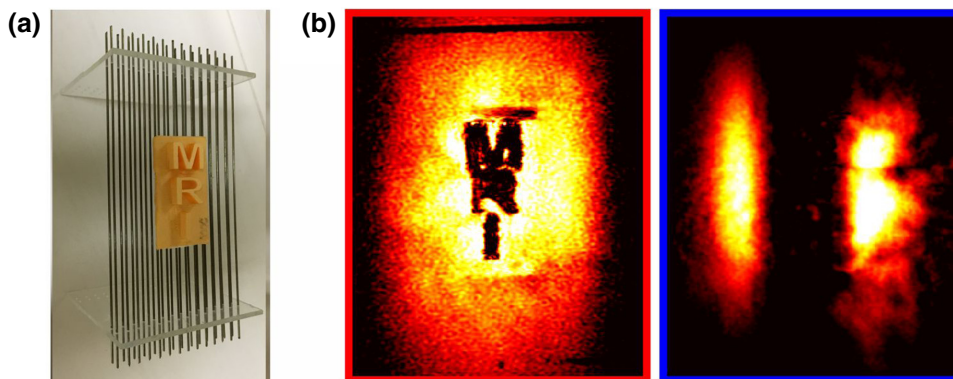

FIG. 3. (a) Photograph of the experimental setup: three-dimensional "MRI" word made from Styrofoam material is placed on top of the metasurface in the center. (b) Measured image intensities acquired with the metasurface tuned close to the first (left) and second (right) eigenmodes.

adiabatic pulses to overcome the variable B_1^+ field or use detunable metasurfaces that are only active during signal reception. While we have considered only a flat metallic metasurface design, all-dielectric structures, e.g., water-based dielectric metasurfaces supporting anapole states [33] or metamaterial-based spheres [34], can be studied within the MRI scanner.

ACKNOWLEDGMENTS

[1] N. Engheta and R. W. Ziolkowski, *Metamaterials: Physics and Engineering Explorations* (Wiley-IEEE Press, Piscataway, 2006).

[2] S. Glybovski, S. Tretyakov, P. Belov, Y. Kivshar, and C. Simovski, Metasurfaces: From microwaves to visible, Phys. Rep. **634**, 1 (2016).

[3] J. Pendry, Manipulating the near field with metamaterials, Opt. Photon. News **15**, 32 (2004).

[4] A. Ishikawa, S. Zhang, D. Genov, G. Bartal, and X. Zhang, Deep Subwavelength Terahertz Waveguides Using gap Magnetic Plasmon, Phys. Rev. Lett. **102**, 043904 (2009).

[5] F. Lemoult, N. Kaina, M. Fink, and G. Lerosey, Wave propagation control at the deep subwavelength scale in metamaterials, Nat. Phys. **9**, 55 (2012).

[6] N. Kaina, A. Causier, Y. Bourlier, M. Fink, T. Berthelot, and G. Lerosey, Slow waves in locally resonant metamaterials line defect waveguides, Sci. Rep. **7**, 15105 (2017).

[7] X. Cheng, C. Jouvaud, X. Ni, S. H. Mousavi, A. Z. Genack, and A. B. Khanikaev, Robust reconfigurable electromagnetic pathways within a photonic topological insulator, Nat. Mater. **15**, 542 (2016).

[8] I. Liberal, A. M. Mahmoud, and N. Engheta, Geometry-invariant resonant cavities, Nat. Commun. **7**, 10989 (2016).

[9] F. Lemoult, G. Lerosey, J. d. Rosny, and M. Fink, Resonant Metalenses for Breaking the Diffraction Barrier, Phys. Rev. Lett. **104**, 203901 (2010).

[10] J. Yao, X. Yang, X. Yin, G. Bartal, and X. Zhang, Three-dimensional nanometer-scale optical cavities of indefinite medium, Proc. Natl Acad. Sci. USA **108**, 11327 (2011).

[11] A. E. Miroshnichenko, D. Filonov, B. Lukyanchuk, and Y. Kivshar, Antiferromagnetic order in hybrid electromagnetic metamaterials, New J. Phys. **19**, 083013 (2017).

[12] A. B. Khanikaev, N. Arju, Z. Fan, D. Purtseladze, F. Lu, J. Lee, P. Sarriugarte, M. Schnell, R. Hillenbrand, M. A. Belkin, and G. Shvets, Experimental demonstration of the microscopic origin of circular dichroism in two-dimensional metamaterials, Nat. Commun. **7**, 12045 (2016).

[13] N. Rotenberg and L. Kuipers, Mapping nanoscale light fields, Nat. Photon. **8**, 919 (2014).

[14] H. Wen, F. A. Jaffer, T. J. Denison, S. Duewell, A. S. Chesnick, and R. S. Balaban, The evaluation of dielectric resonators containing H_2O or D_2O as RF coils for high-field MR imaging and spectroscopy, J. Magn. Reson. B **110**, 117 (1996).

[15] A. Webb, Visualization and characterization of pure and coupled modes in water-based dielectric resonators on a human 7T scanner, J. Magn. Reson. **216**, 107 (2012).

[16] A. Tonyushkin, D. Deelchand, P. Van de Moortele, G. Adriany, and A. Kiruluta, Direct imaging of radio-frequency modes via traveling wave magnetic resonance imaging, J. Appl. Phys. **119**, 024904 (2016).

[17] W. R. Hendee, Physics and applications of medical imaging, Rev. Mod. Phys. **71**, 444 (1999).

[18] E. Georget, M. Luong, A. Vignaud, E. Giacomini, E. Chazel, G. Ferrand, A. Amadon, F. Mauconduit, S. Enoch, G. Tayeb, N. Bonod, C. Poupon, and R. Abdeddaim, Stacked magnetic resonators for MRI RF coils decoupling, J. Magn. Reson. **275**, 11 (2017).

[19] M. J. Freire, L. Jelinek, R. Marques, and M. Lapine, On the applications of $\mu = -1$ metamaterial lenses for magnetic resonance imaging, J. Magn. Reson. **203**, 81 (2010).

[20] M. Dubois, L. Leroi, Z. Raolison, R. Abdeddaim, T. Antonakakis, J. de Rosny, A. Vignaud, P. Sabouroux, E. Georget, B. Larrat, G. Tayeb, N. Bonod, A. Amadon, F. Mauconduit, C. Poupon, D. Le Bihan, and S. Enoch, Kerker Effect in Ultrahigh-Field Magnetic Resonance Imaging, Phys. Rev. X **8**, 031083 (2018).

[21] G. Duan, X. Zhao, S. W. Anderson, and X. Zhang, Boosting magnetic resonance imaging signal-to-noise ratio using magnetic metamaterials, Commun. Phys. **35**, 2 (2019).

[22] C. Jouvaud, R. Abdeddaim, B. Larrat, and J. de Rosny, Volume coil based on hybridized resonators for magnetic resonance imaging, Appl. Phys. Lett. **108**, 023503 (2016).

[23] C. Rizza, M. Fantasia, E. Palange, M. Alecci, and A. Galante, Harnessing Surface Plasmons for Magnetic Resonance Imaging Applications, Phys. Rev. Appl. **12**, 044023 (2019).

[24] A. P. Slobozhanyuk, A. N. Poddubny, A. J. E. Raaijmakers, C. A. T. van den Berg, A. V. Kozachenko, I. A. Dubrovina, I. V. Melchakova, Y. S. Kivshar, and P. A. Belov, Enhancement of magnetic resonance imaging, Adv. Mater. **28**, 1832 (2016).

[25] R. Schmidt, A. Slobozhanyuk, P. Belov, and A. Webb, Flexible and compact hybrid metasurfaces for enhanced ultra high field in vivo magnetic resonance imaging, Sci. Rep. **7**, 1678 (2017).

[26] J. M. Algarin, M. A. Lopez, M. J. Freire, and R. Marques, Signal-to-noise ratio evaluation in resonant ring metamaterial lenses for MRI applications, New J. Phys. **13**, 115006 (2011).

[27] M. A. Lopez, M. J. Freire, J. M. Algarin, V. C. Behr, P. M. Jakob, and R. Marqués, Nonlinear split-ring metamaterial slabs for magnetic resonance imaging, Appl. Phys. Lett. **98**, 133508 (2011).

[28] See Supplemental Material at http://link.aps.org/supplemental/10.1103/PhysRevApplied.16.L021002 for details about the numerical simulations, experiments, and eigenmodes of the metasurface.

[29] W. J. Ellison, K. Lamkaouchi, and J.-M. Moreau, Water: A dielectric reference, J. Mol. Liq. **68**, 171 (1996).

[30] A. Andryieuski, S. M. Kuznetsova, S. V. Zhukovsky, Y. S. Kivshar, and A. V. Lavrinenko, Water: Promising opportunities for tunable all-dielectric electromagnetic metamaterials, Sci. Rep. **5**, 13535 (2015).

[31] J. Vaughan and J. Griffiths, *RF Coils for MRI* (Wiley, New York, 2012).

[32] A. V. Shchelokova, A. P. Slobozhanyuk, I. V. Melchakova, S. B. Glybovski, A. G. Webb, Y. S. Kivshar, and P. A. Belov, Locally Enhanced Image Quality with Tunable Hybrid Metasurfaces, Phys. Rev. Appl. **9**, 014020 (2018).

[33] E. Takou, A. C. Tasolamprou, O. Tsilipakos, Z. Viskadourakis, M. Kafesaki, G. Kenanakis, and E. N. Economou, Anapole Tolerance to Dissipation Losses in Thermally Tunable Water-Based Metasurfaces, Phys. Rev. Appl. **15**, 014043 (2021).

[34] C. Rizza, E. Palange, M. Alecci, and A. Galante, Mimicking Localized Surface Plasmons via Mie Resonances to Enhance Magnetic-Resonance-Imaging Applications, Phys. Rev. Appl. **14**, 034040 (2020).